Available online at www.sciencedirect.com
SCIENCE DIRECT®
International Journal of Heat and Fluid Flow 24 (2003) 520–528
International Journal of HEAT AND FLUID FLOW
www.elsevier.com/locate/ijhff

Analysis of a jet–mixing layer interaction

S. Lardeau [a,*], E. Collin [b], E. Lamballais [b], J.P. Bonnet [b]

[a] Department of Aeronautics, Imperial College of Science, Technology and Medicine, Prince Consort Road, South Kensington, London SW7 2BY, UK
[b] Laboratoire d'Etudes Aérodynamiques, C.E.A.T.—Université de Poitiers 43, rue de l'Aérodrome, F 86036 Poitiers Cedex, France

Received 23 November 2002; accepted 19 March 2003

Abstract

The improvement of mixing in free-shear flows via external jets has been proven efficient in subsonic and supersonic flows as well. However, the hyper-mixing process is not well known. The present study deals with an experimental and a numerical approach of the interaction of an external control jet with a turbulent mixing layer. The main conclusion is that an intermittent penetration of the control jet occurs both in supersonic and subsonic configurations. Moreover, all results tend to show that the control jet flapping frequency and the spacing between the structures involved downstream of the interaction are respectively very close to the frequency and wavelength of the Kelvin–Helmholtz structures at the impact location. Two hypotheses are provided in order to explain the mechanism of the interaction. The first one is based upon the interaction with the passage of Kelvin–Helmholtz structures in the mixing layer, the other deals with an intrinsic instability of such a flow configuration.

Keywords: Jet; Mixing enhancement; Pneumatic actuators; Direct numerical simulation; Supersonic flows; Visualizations; Coherent structures

1. Introduction

In many industrial applications, especially in ejectors and propulsive jets, most of the dynamical behavior of the system is strongly influenced by the mixing efficiency in the jet. This is particularly the case when dilution of hot propulsive jets is required, for example to reduce the infrared signature of a military aircraft. Many control strategies have been proposed to improve the mixing efficiency of free-shear flows, from the very simple but very efficient method of small *tabs* placed at the nozzle exit to more sophisticated approaches like MEMS or synthetic jets. The control of supersonic jets can also be performed through pneumatic devices, which are generally preferred to mechanical devices for these regimes. It is admitted that transverse jets, like the *tabs*, generate longitudinal vorticity in a cross flow. The improvement to mixing in jets via small external jets is very efficient both for subsonic and supersonic flows (Davis, 1982; Delville et al., 2000; Freund and Moin, 2000; Lardeau et al., 2002). However, the hyper-mixing process seems to occur only in the very near field region of the impact between the control jet (CJ) and the main mixing layer (Lardeau et al., 2002). This limited effect is also observed when mechanical actuators are used (Bradbury and Khadem, 1975).

The objective of the work presented here is to characterize the flow in the very near field of a CJ impacting on a main mixing layer. Two very different flow configurations have been studied. In the first one, a supersonic/subsonic mixing layer is controlled by a supersonic rectangular CJ. In the second configuration, an incompressible plane mixing layer is controlled by a round CJ. The intention, through this dual study, is to analyze an intermittent penetration phenomenon originally observed experimentally in the supersonic configuration. The complexity of the flow configuration leads to difficulties in the measurements and in the simulations. Although compressibility and Reynolds number effects cannot be neglected, we demonstrate that the CJ intermittent penetration observed in the experiments can also be observed numerically in a much simpler configuration. Initially, the experiment and the simulation were performed separately, and it was not expected to

* Corresponding author. Tel.: +44-207-594-5129; fax: +44-207-584-8120.
E-mail address: s.lardeau@imperial.ac.uk (S. Lardeau).

0142-727X/03/$ - see front matter © 2003 Elsevier Science Inc. All rights reserved.
doi:10.1016/S0142-727X(03)00046-8

Nomenclature

CJ	control jet	U_{CJ}	centerline control jet velocity
DNS	direct numerical simulation	x	streamwise direction
D	diameter of the main jet (experiment)	y	transverse direction
M_c	convective Mach Number	z	spanwise direction
G'	fluctuating grayscale level	δ_ω	vorticity thickness of the mixing layer
Re_{δ_ω}	Reynolds number based on the vorticity thickness	λ_{KH}	wavelength of the Kelvin–Helmholtz structures
R_{GG}	autocorrelation function of the fluctuating grayscale level	λ	velocity ratio, $\lambda = (U_1 - U_2)/(U_1 + U_2)$
St	Strouhal number	ϕ	angle between the streamwise direction and the direction of the CJ
U_1	centerline main jet velocity	Ω	symmetric part of the velocity gradient tensor
U_2	co-flow velocity	S	antisymmetric part of the velocity gradient tensor
U_c	convective velocity, $U_c = (U_1 + U_2)/2$		

observe similar phenomena. Hence, a direct comparison of the results is not straightforward, and the differences must be discussed very carefully.

In the experiment, it is clear that compressibility effects are influential on the flow development, providing that the convective Mach number M_c is equal to 0.49. The present DNSs do not take the compressible character of the flow into account. Experimental evidence of such effects has been historically recorded by Papamoschou and Roshko (1988), and specific effects for this flow have been measured by Barre et al. (1994). DNSs at the same convective Mach number have been performed by Sandham and Reynolds (1991). Recent DNS results, by Pantano and Sarkar (2002), are in good agreement with the experiment of Barre et al. (1994). The major effects have been observed on the repartition of the energy among the different component of the Reynolds stress tensor. It has also been shown by Samimy et al. (1992) that compressibility can act upon the structural organization of the mixing layer. Under compressibility effects, the organization of the large-scale structures becomes three dimensional, with strong oblique regions of rotation. The Reynolds number considered in the present DNS is significantly lower than in the experiment. The Reynolds number, based on the local vorticity thickness, is of the order of 10^5 in the experiment and is equal to 200 in the simulations. Despite this difference, it is reasonable to assume that, for a first analysis, the large-scale physical processes involved in the CJ/main flow interaction are not strongly dependant on viscous effects. This point will be confirmed here by important qualitative similarities between numerical and experimental results.

The third difference is the inclination with respect to the streamwise direction of the CJ. In the DNS, the jet is inclined at an angle $\phi = 45°$, whereas in the experiment the CJ impacts perpendicularly with the shear layer. The angle ϕ is imposed by the numerical method used to solve the Navier–Stokes equations and its possible effects have been discussed in Lardeau et al. (2002). The geometry of the CJ also differs between the experiment and the computations. When practical applications are concerned, the cost efficiency is one of the most important factors. By using a rectangular CJ in the experiment, the goal is to remain as close as possible to a practical configuration. In a previous study, Denis (2000) has shown that the same cost efficiency can be obtained when either rectangular or round CJ are used. She also determined that the position (with respect to the main jet nozzle) and the velocity of the CJ are the two more important parameters involved in increasing the mixing efficiency. However, this type of geometry implies an increase of the computational cost, more grid points being needed to accurately describe a rectangular jet.

The manipulated mixing layer also differs between the experimental and the numerical studies. The main flow in the experiment is a round jet whereas in the DNS it is a plane mixing layer. Nevertheless, in the experimental study, the ratio δ_ω/D (where D is the main jet diameter and δ_ω is the vorticity thickness of the mixing layer) is about 0.1 in the impact region. This ratio is small enough to let us suppose that curvature effects do not strongly influence the phenomenon studied. Considering the discrepancies between the experimental and numerical conditions, the major purpose of this paper is then only to extract the global features of the jets interaction, irrespective to the compressible nature of the flow, Reynolds number effects, the CJ angle of attack and geometry. Previous simulations and experiments have shown that the velocity ratio λ has a strong effect on the development of a mixing layer (see Bonnet et al., 1998, for a recent review). Indeed, the values of the velocity ratio λ in both of the present studies are very close

($\lambda = 0.78$ in the experiment and $\lambda = 0.83$ in the simulations) which may help to compare results.

The first part of this paper deals with an experimental approach of the interaction of an external supersonic CJ with a turbulent supersonic/subsonic mixing layer. These results are then compared in the second part to results obtained by direct numerical simulation (DNS) of an incompressible mixing layer controlled by a round jet.

2. Experimental study

The experimental study aims at getting a better knowledge of the flow characteristics in a supersonic regime, which is as close as possible to the conditions of a mixing enhancement device devoted to reduce the infrared signature of military aircrafts.

2.1. Experimental set-up

The wind tunnel used in this study is the S150 high-pressure facility of the C.E.A.T. of Poitiers, France. This is an $M = 1.37$ supersonic jet surrounded by a subsonic entrained co-flow. Stagnation pressure and temperature for the main jet are respectively 3 bar and 260 K. The co-flow velocity and stagnation temperature are 47 $\mathrm{m\,s^{-1}}$ and 290 K. The convective Mach number is $M_c = 0.49$. The supersonic jet has the same static pressure as the subsonic co-flow. The nozzle diameter is $D = 50$ mm. The test section is 500×500 mm^2. A 200 bar dry air tank supplies the main jet.

The CJ is supplied by the same 200 bar dry air tank as the main jet and is placed at $D/10$ downstream and $D/10$ bellow the main jet nozzle as shown in Fig. 1. The CJ stagnation pressure is kept constant at 2.5 bar, which involves a velocity ratio $U_{CJ}/U_1 = 0.89$. Fig. 2 shows the test section. The CJ is seeded with SiO_2 particles.

Visualizations of the flow are obtained with a PIV system. A laser sheet is realized with an Nd YAG pulsed laser beam. Here, the laser sheet is positioned in the symmetry plane of the main jet. Pictures are acquired on computer by the use of a CCD camera. The time of exposure is about 8 ns, which is short enough to 'freeze' the flow. Side views are easily performed thanks to large windows in the walls of the test section. We acquire 200 instantaneous pictures at 10 Hz. Each picture has 768×484 pixels, coded on 256 grayscale levels. Simple algorithms give well-converged average and rms pictures for each run.

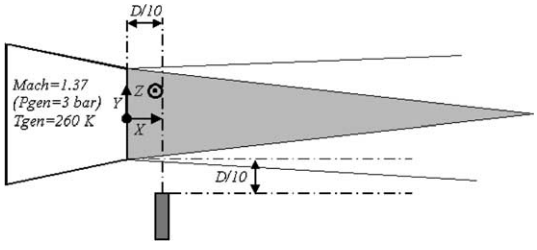

Fig. 1. Flow arrangement.

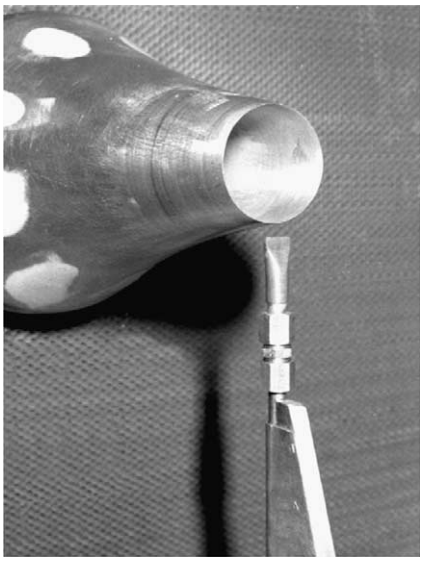

Fig. 2. Photography of the test section.

2.2. Results

Fig. 3 shows the averaged and rms pictures obtained using the 200 instantaneous pictures. The main flow direction is from left to right. The trajectory of the CJ looks like the one obtained with jets in cross flow. However, the curvature seems to be much more important in the region where the CJ is impinging on the main supersonic jet, and the CJ spreads downward. The

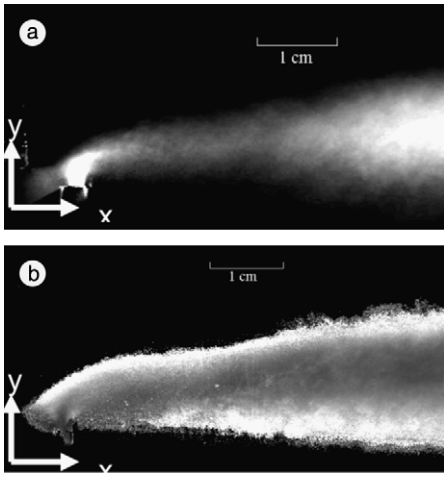

Fig. 3. (a) Average and (b) rms pictures of the seeded CJ impacting the main mixing layer.

averaged picture shows also that the CJ turns into the mixing layer.

The rms side view indicates that the boundaries of the CJ are turbulent. We can also notice that a part of the CJ turns upstream, very near the CJ nozzle. This behavior is better understood in the analysis of the instantaneous pictures.

Close-up instantaneous views are represented in Fig. 4. We can see that two kinds of behavior occur: either the CJ penetrates deeply into the mixing layer, or it is completely stopped when it reaches the mixing layer. The CJ intermittent penetration involves the formation of quasi-2D large-scale structures downstream, in the manipulated mixing layer, as shown in Fig. 5, where a comparison between the lower (manipulated) and the upper (not influenced) sides of the main jet is given.

The wavelength associated with these large-scale and well-organized structures can be evaluated via the autocorrelation function $R_{GG}(\Delta x)$, defined as

$$R_{GG}(\Delta x) = \overline{\left[\frac{\langle G'(x,y(x))\cdot G'(x+\Delta x),y(x+\Delta x)\rangle}{\langle G'(x,y(x))^2\rangle}\right]} \quad (1)$$

where G' is the fluctuating grayscale level in the (x,y)-plane, $\langle * \rangle$ represents the average over x, $\overline{(*)}$ represents the average over the 200 instantaneous pictures, and

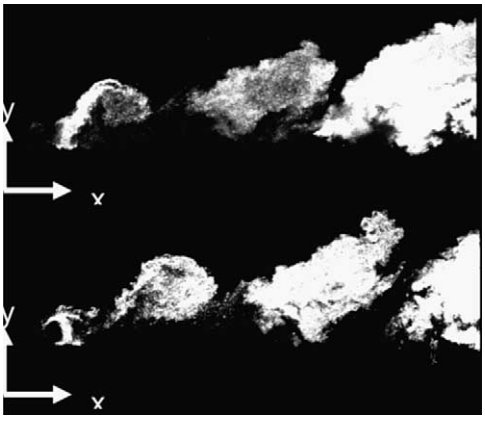

Fig. 4. Instantaneous side views of the structures of the CJ.

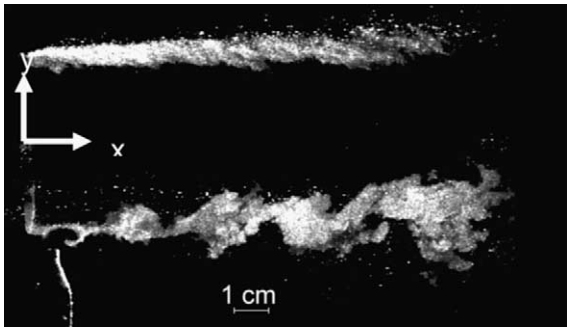

Fig. 5. Instantaneous side view of the seeded main mixing layer controlled by the CJ.

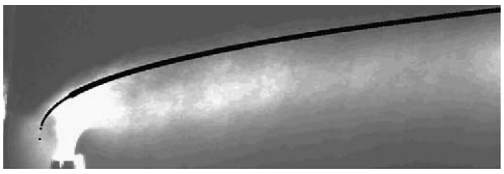

Fig. 6. Description of the CJ upstream boundary.

$y(x)$ describes the CJ upstream boundary as it appears on the average picture (see Fig. 6).

The autocorrelation function obtained from the CJ seeded pictures is shown in Fig. 7. It appears that the large-scale structures wavelength is approximately $\lambda = 25$ mm. This value is very close to λ_{KH}, the Kelvin–Helmholtz structures spacing of the non-manipulated main mixing layer (at the impact location). In the near field of interaction, assuming that

$$St = f\cdot\delta_\omega/U_c = \delta_\omega/\lambda_{KH} = 0.2 \quad (2)$$

we can estimate the wavelength of the Kelvin–Helmholtz vortices as $\lambda_{KH} = 25$ mm. Assuming now that the structures in the manipulated mixing layer propagate downstream at the natural convective velocity ($U_c = 230$ m s^{-1}), the frequency associated with the CJ flapping is typically of the order of the frequency associated with the non-manipulated main mixing layer structures.

Since the mechanism responsible of the CJ intermittent penetration is not well known, we propose two hypotheses. First, as the CJ size is quite small, it is possible that the penetration depends on the presence of a Kelvin–Helmholtz structure in front of the CJ exit. Indeed, if the adverse pressure gradient were sufficiently strong just upstream of a Kelvin–Helmholtz rollup, the penetration of the CJ would decay. On the other hand, when the CJ nozzle is behind a Kelvin–Helmholtz rollup, the penetration is enhanced. A schematic description of this hypothesis is given in Fig. 8a. However, this mechanism implies that the Kelvin–Helmholtz rollups generate very strong pressure fluctuations.

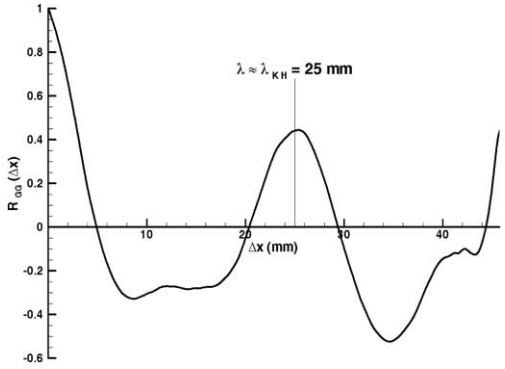

Fig. 7. Autocorrelation function of grayscale levels for extracted horizontal lines of the CJ seeded pictures.

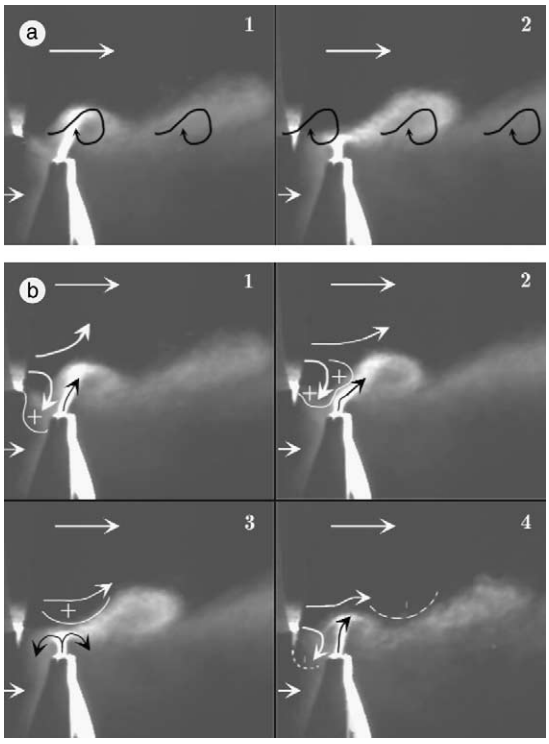

Fig. 8. Schematic description of the two mechanisms responsible for the CJ penetration intermittency.

The other hypothesis is based on an intrinsic instability of the interaction between the CJ and the annular mixing layer. This instability may be due to the generation of a high-pressure region just upstream of the CJ, caused by a local downward deviation of the main jet. When the pressure upstream of the CJ is sufficiently strong (i.e. at least equal to the CJ stagnation pressure), the high-pressure zone is convected downstream, stopping the penetration of the CJ. Fig. 8b illustrates this hypothesis. Unfortunately, we need further measurements or simulations in this way to confirm if the intermittent penetration behavior is due to this kind of mechanism.

An additional comment should be made concerning the second hypothesis: since a portion of high-speed fluid seems to be deviated downward, just along the upward CJ stream, an absolute instability (AI) could play a significant role in the CJ destabilization process. Recent non-intrusive velocity measurements just upstream of the CJ (Collin, 2001) indicate that the AI threshold (Huerre and Monkewitz, 1985) may have been crossed in this region of the flow.

3. Numerical study

Some DNSs have been performed in a simplified flow configuration. We have already stressed in the introduction that the two flow configurations are very different. Nevertheless, these differences are supposed to have a weak effect on the intermittency penetration of the CJ in the mixing layer of the main flow. Moreover, the two hypotheses proposed in the previous part to explain this phenomenon do not involve any compressibility effect. The flow in the following DNS is incompressible. We also introduce a second modification: because the curvature does not seem to be very important near the impact region, and because in the experiment the CJ are small enough compare to the size of the main jet, the main annular mixing layer is approximated as a plane mixing layer, in order to reduce the computational cost. These assumptions do not have a fundamental impact on the results. The same intermittent behavior has been observed in previous computation of the control of a round jet by CJ, for a diameter ratio between the CJ and the main jet much higher (Lardeau et al., 2002).

3.1. Flow configuration and numerical methods

In this part, we consider the interaction between an inclined jet and a mixing layer in a Cartesian frame of reference $(Oxyz)$, x, y, z are respectively the streamwise, transverse and spanwise directions (Fig. 9). u_x, u_y and u_z are the velocity components. A free-slip condition is imposed in the transverse y-direction and a periodic boundary condition is used in the spanwise direction. The outflow condition is deduced by solving a simplified convective equation.

At the inflow section, the control jet is inclined by an angle of $\phi = 45°$. In the computation presented below, the inflow mean velocity profile $u_x(y)$ is given by a hyperbolic tangent with

$$u_x(y) = \frac{1}{2}\left[(U_1 + U_2) + U\tanh\left(\frac{2y}{\delta_{\omega i}}\right)\right] \tag{3}$$

where $\delta_{\omega i}$ is the inflow vorticity thickness, U_1 and U_2 are respectively the high- and low-speed free-stream velocities and $U = U_1 - U_2$ is the velocity difference. The

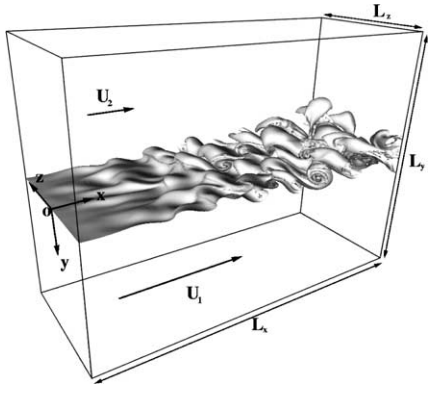

Fig. 9. Computational domain and axis.

Table 1
Flow configuration and simulation parameters

Designation	(Lx, Ly, Lz)	(nx, ny, nz)	U_1	U_2
Laminar	$(122\delta_{\omega t}, 86.4\delta_{\omega t}, 43.2\delta_{\omega t})$	(245, 289, 144)	$1.05U$	$0.05U$
Turbulent	$(96\delta_{\omega t}, 216\delta_{\omega t}, 36\delta_{\omega t})$	(193, 865, 144)	$1.10U$	$0.10U$

parameter associated with the main flow is the Reynolds number $Re = U\delta_\omega/\nu$.

The incompressible Navier–Stokes equations are directly solved using a non-staggered grid. Sixth order compact centered difference schemes are used (Lele, 1992) to evaluate all spatial-derivatives, except near the in- and out-flow boundaries, where single sided schemes are employed for the x-derivative calculation. Time integration is performed with a third order Runge–Kutta method. To study control effects on mixing properties, an additional passive scalar equation is solved (see Lardeau et al. (2002), for details about the code).

Two types of flow are studied: first, we consider the control of a mixing layer with two-dimensional Kelvin–Helmholtz vortices (referenced in the following as the "laminar" simulation). The interaction between the control jet and a turbulent mixing layer (referenced as "turbulent") is studied in the second part of this work. The main parameters for these two simulations are shown in Table 1.

3.2. Control of the two-dimensional structures of a mixing layer

We consider first the control of an initially two-dimensional mixing layer by a control jet. To generate the mixing rollup at a given frequency, an harmonic perturbation is superimposed to the u_y-component of the velocity field. The Strouhal number, defined as $St = f_0\delta_{\omega t}/U$, is equal to $St = 0.066$ and the Reynolds number, based on the inflow vorticity thickness $\delta_{\omega t}$ is equal to 200. By comparison, the Reynolds number of the experiment, based on the local vorticity thickness near the impact region is equal to $Re = 10^5$. In this simulation, the u_z-component of the velocity field is set equal to zero, as well as the derivative in the z-direction

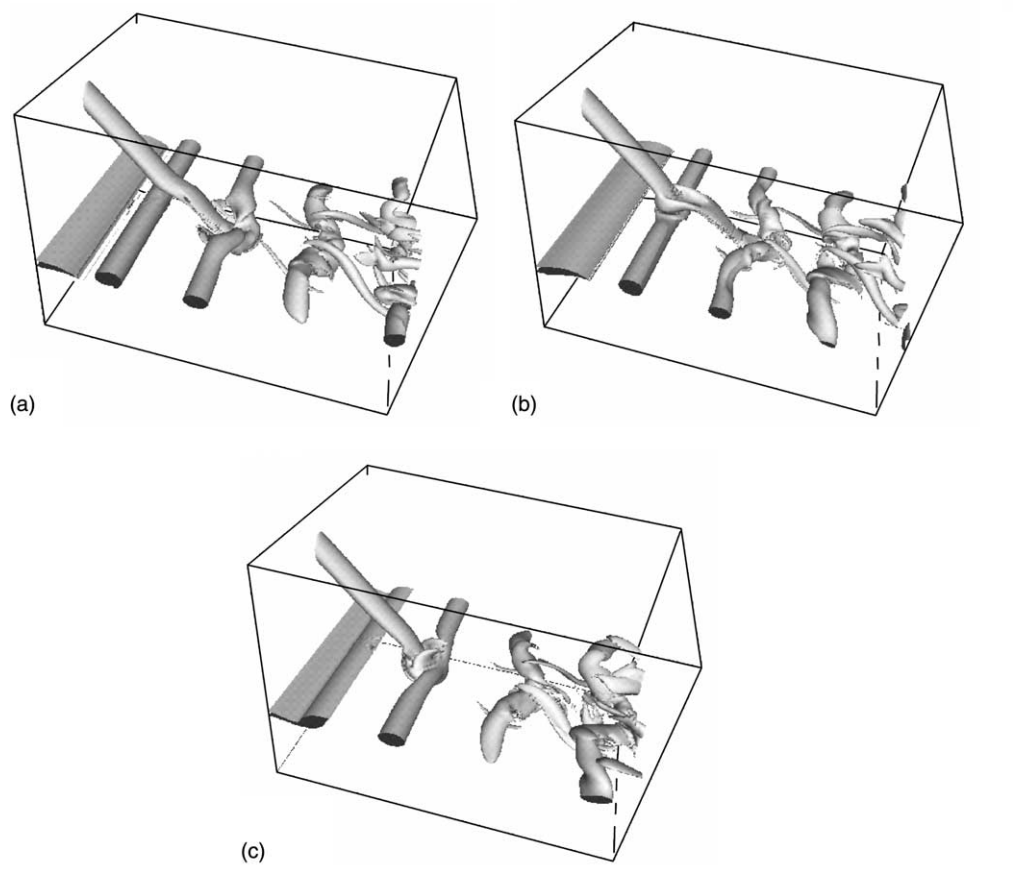

Fig. 10. Iso-surfaces of vorticity modulus for $\|\omega\| = 0.5U/\delta_{\omega t}$: (a) $t = 202.7\delta_{\omega t}/U$; (b) $t = 211.8\delta_{\omega t}/U$; (c) $t = 221.9\delta_{\omega t}/U$.

and the control jet velocity U_{CJ} is set equal to the high-speed stream velocity. Fig. 10 shows of iso-surfaces of the vorticity modulus for the "laminar" simulation. The different views correspond to three consecutive positions for the same Kelvin–Helmholtz vortex. Only the region near the impact is shown on this figure.

As mentioned in the first part of this work, an intermittent penetration of the control jet into the high-speed stream side of the mixing layer can be observed near the impact region. When the eddy is upstream of the impact region (Fig. 10a), the control jet cannot penetrate the shear layer and is deviated downstream, in the same manner as on Fig. 4 (left). When the vortex crosses the Kelvin–Helmholtz structure (Fig. 10b) the jet can enter the eddy. Then the control jet winds around the two-dimensional vortex (Fig. 10c). The control jet is only slightly deviated upstream, due to the inclination of the CJ, but this picture shows a similar behavior to that on Fig. 4 (right). Downstream from the impact region, the control process immediately involves fully non-linear interaction between the main flow and the actuation itself, the flow becomes fully turbulent. These observations show that in this case the intermittent behavior observed above is clearly related to the passage of a Kelvin–Helmholtz structure.

3.3. Control of a turbulent mixing layer

Now we consider the control of a turbulent mixing layer. To generate the turbulent mixing layer, small random perturbations with a prescribed kinetic energy spectrum are superimposed on the three components of the velocity field. In contrast with the use of a conventional white noise, the prescription of spectral energy generates spatially correlated inflow data that can be accurately resolved by the computational grid near the inlet. The use of this set of inflow conditions allows one to mimic approximately the residual turbulence concentrated in the shear region and created experimentally by the boundary layers upstream of the leading edge of the splitter plate. In the case presented below, the high- and low-speed stream velocities are $U_1 = 1.1U$ and $U_2 = 0.1U$ respectively, and the control jet velocity is equal to $U_{CJ} = 1.5U$. The Reynolds number, based on the inflow vorticity thickness of the shear layer is equal to $Re = 200$. Iso-surface of vorticity modulus is presented on Fig. 11. The organization of coherent structures is strongly affected by the fluid injection, with the creation of large-scale vortices downstream from the impact.

Fig. 12 shows the vertical velocity component u_y in the *Oxy* plane for two different instants. The CJ velocity is represented in black. As mentioned in the experimental part, an intermittent penetration is clearly observed, but unlike the "laminar" case, there are no well-defined Kelvin–Helmholtz vortices in the mixing layer upstream of the impact region (see Fig. 4 for a comparison). Again, the upstream deviation of the CJ is not very important, due the inclination of the CJ.

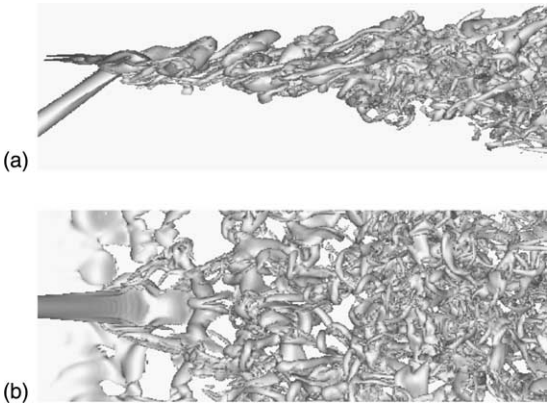

Fig. 11. Vorticity modulus iso-surface $\|\omega\| = 0.5U/\delta_{\omega t}$ in the (a) *Oxy* plane and (b) *Oxz* plane.

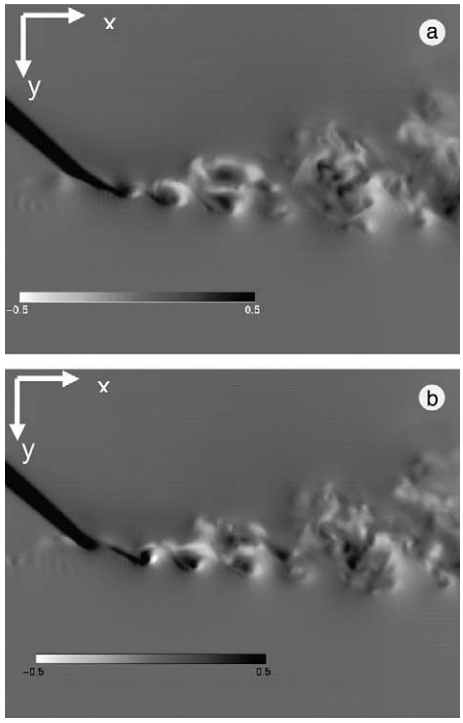

Fig. 12. Vertical velocity in the *Oxy* plane for the turbulent simulation: (a) $t = 1308.6\delta_{\omega t}/U$; (b) $t = 1315.8\delta_{\omega t}/U$.

Another phenomenon is observed in the transverse direction. Fig. 13 shows a cross section of the scalar field in the *Oxz* plane for two different instants (the same moments as in Fig. 12). Animations of the flow show that vortices of opposite rotation form systematically in phase downstream from the impact region. These vortices are similar to those created in the wake of a cylinder submitted to a sudden displacement (Coutanceau and Bouard, 1977).

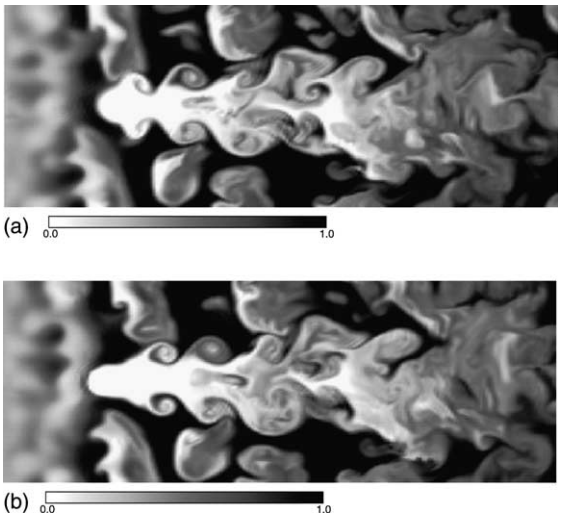

Fig. 13. Planar view of the scalar field in the *Oxz* plane for the turbulent simulation: (a) $t = 1308.6\delta_{\omega 1}/U$; (b) $t = 1315.8\delta_{\omega 1}/U$.

The frequencies of these two phenomena (signatures of wake and Kelvin–Helmholtz-like vortices in *Oxz* and *Oxy* planes respectively) are equal to the preferred frequency of the shear layer. In order to link the vortical structures created downstream from the impact region, Fig. 14 shows iso-surfaces of the *Q*-criterion, defined as

$$Q = \frac{1}{2}(\|\Omega\|^2 - \|S\|^2) \tag{4}$$

where Ω and S are respectively the symmetric and antisymmetric part of the velocity gradient tensor (Dubief and Delcayre (2000)). The region near the impact has been magnified. In order to confirm the link between the *Oxy* and *Oxz* views, Fig. 14 also shows the two planes. The 3D visualization allows us to identify clearly the periodic creation of horseshoe vortices leading to the appearance of a Kelvin–Helmholtz structure in its vertical symmetry plane, and two wake vortices in the horizontal plane. The link between these highly 3D large-scale structures and their 2D signature in *Oxy* and *Oxz* planes is clearly shown by the two maps of the scalar fields presented on Fig. 14 at the same instant. When convected, this horseshoe structure is stretched by the velocity gradient. Further downstream, the flow becomes fully turbulent, and only few pairing of such structures can be observed (Fig. 11). Note that these structures are also similar to some extent to the structures observed in the 2D simulation, in Fig. 10c for instance.

4. Conclusion

The CJ penetration intermittency, experimentally detected in a supersonic regime, has been reproduced numerically in a much simpler configuration. On one hand, it has been demonstrated that the presence of well-organized Kelvin–Helmholtz rollups can interact with the control jet. On the other hand, this intermittent behavior has also been observed for a turbulent (less organized) mixing layer. This implies that both the hypotheses proposed are valuable: the CJ may interact with the Kelvin–Helmholtz structures, but the flow does not have to be well organized to reproduce this phenomenon. A complex mechanism involving the Kelvin–Helmholtz rollups, a CJ intrinsic instability and an absolute instability could explain the intermittency.

Whatever causes the intermittency, the result is the development of large-scale structures in the manipulated mixing layer downstream of the impact region. The Strouhal number associated with these vortices is close to the natural mixing layer Strouhal number. The numerical study brings out the mixing layer structure geometry downstream of the impact. The main effect of the CJ is to produce horseshoe quasi-symmetrical vortices, these vortices being elongated by the mean shear of the mixing layer.

The question of the compressibility effect on the intermittent penetration of the CJ requires further study, the stabilizing effect of the compressibility being more important as the convective Mach number increased. On one hand, future work will concern the parametric study of the CJ intermittent penetration. This will focus on the effects of the CJ geometry, the CJ velocity ratio, and the main mixing layer velocity ratio. We expect to evaluate the flow regimes in which the intermittency occurs, and

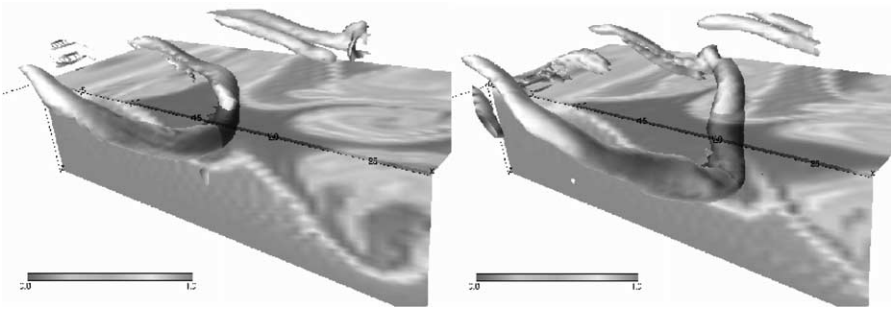

Fig. 14. *Q*-criterion iso-surface $Q = 0.5U^2/\delta_{\omega 1}^2$.

to determine the link between the CJ flapping and the Kelvin–Helmholtz frequencies. On the other hand, particle imaging velocity measurements will be realized in order to explore the hypothesis involving an absolute instability between the CJ upstream boundary and the flow deviated downward.

Acknowledgement

Computations were carried out at the Institut du Développement et des Ressources en Informatique scientifique (IDRIS), the computational center of the Centre National de la Recherche Scientifique (CNRS).

References

Barre, S., Quine, C., Dussauge, J.P., 1994. Compressibility effects on the structure of supersonic mixing layers: experimental results. J. Fluid Mech. 259, 47–78.

Bonnet, J.P., Moser, R., Rodi, W. 1998. Free-shear flows. A Selection of Test Cases for Validation of Large-eddy Simulations of Turbulent Flows 245, 29–35.

Bradbury, L.J., Khadem, A.H., 1975. The distortion of jet by tabs. J. Fluid Mech. 70, 801–813.

Collin, E., 2001. Etude de l'injection radiale de fluide dans une couche de mélange annulaire supersonique, application à l'augmentation du mélange (Study of a radial fluid injection into a supersonic annular mixing layer, mixing enhancement application). PhD dissertation, Université de Poitiers, France.

Coutanceau, M., Bouard, R., 1977. Experimental determination of the main features of the viscous flow in the wake of a circular cylinder in uniform translation. Part 2: Unsteady flow. J. Fluid Mech. 79, 257–272.

Davis, M.R., 1982. Variable control of jet decay. AIAA J. 20 (5), 606–609.

Delville, J., Collin, E., Lardeau, S., Lamballais, E., Barre, S., Bonnet, J.P., 2000. Control of jets by radial fluid injection. ERCOFTAC Bull. 44, 57–67.

Denis, S., 2000. Contrôle du développement des couches de mélanges axisymétriques subsoniques par jets impactants. PhD dissertation. Université de Poitiers, France.

Dubief, Y., Delcayre, F., 2000. On coherent vortex identification in turbulence. J. Turbulence 1, 011.

Freund, J.B., Moin, P., 2000. Jet mixing enhancement by high amplitude fluidic actuation. AIAA J. 38 (10), 1863–1870.

Huerre, P., Monkewitz, P.A., 1985. Absolute and convective instabilities in free shear layers. J. Fluid Mech. 159, 151–168.

Lardeau, S., Lamballais, E., Bonnet, J.P., 2002. Direct numerical simulation of a jet controlled by fluid injection. J. Turbulence 3, 002.

Lele, S.K., 1992. Compact Finite difference schemes with spectral like resolution. J. Comp. Phys. 103, 16–42.

Pantano, C., Sarkar, S., 2002. A study of compressibility effects in the high-speed turbulent shear layer using direct simulation. J. Fluid Mech. 451, 329–371.

Papamoschou, D., Roshko, A., 1988. The compressible turbulent shear layer: an experimental study. J. Fluid Mech. 197, 453–477.

Sandham, N.D., Reynolds, W.C., 1991. Three-dimensional simulation of large eddies in the compressible mixing layer. J. Fluid Mech. 224, 133–158.

Samimy, M., Reeder, M.F., Elliott, G.S., 1992. Compressibility effects on large structures in free shear flows. Phys. Fluids A 4 (6), 864–876.